Short-Range Coherence in the Energy Transfer of Photosynthetic Light-Harvesting Systems

Jonaki Ray

School of Chemical Sciences, University of Illinois, 601 S. Goodwin Avenue, Urbana, Illinois 61801

Nancy Makri*

School of Chemical Sciences, University of Illinois, 601 S. Goodwin Avenue, Urbana, Illinois 61801 and Theoretical and Physical Chemistry Institute, National Hellenic Research Foundation, 48 Vassileos Constantinou Avenue, Athens, Greece 11635

Received: May 24, 1999; In Final Form: August 24, 1999

We employ a simple model for the electronic excitations and the exciton−vibration coupling characterizing the B850 ring of the light-harvesting complex in photosynthetic bacteria to investigate the possibility of coherence in the energy transfer within the system. The structure of the equilibrium density matrix is studied using the path integral formulation of quantum statistical mechanics. The calculated mean coherence length is computed from the average root-mean-square deviation of closed imaginary time paths that are sampled via a Monte Carlo procedure. This procedure allows simultaneous examination of the effects of thermal averaging and dynamic and static disorder in a single calculation. The mean coherence length is found to be about two to three chlorophyll monomers at room temperature. The principal factor responsible for this localization is thermal averaging, although static and dynamic disorder further destabilize extended states. At low temperatures the circular arrangement of the pigments favors coherence with respect to the situation in a linear aggregate. Visual inspection of typical paths offers an intuitive picture of the extent of coherent energy delocalization in biological antenna systems.

I. Introduction

The process of energy transduction in the membranes of photosynthetic bacteria begins with the absorption of visible light by light-harvesting antennas which then funnel the energy into the reaction center.[1−6] The light-harvesting complexes are molecular aggregates composed of several units that contain peptides, chlorophyll molecules, and carotenoids. These building blocks are organized in symmetric structures that assume the shape of a ring. The light-harvesting complex I (LH-I) immediately surrounds the reaction center, while a second type of light-harvesting complex (LH-II) channels energy to the reaction center through LH-I.

The structure and electronic arrangement of *Rps. acidophila* and *Rs. molischianum* were determined in recent experimental and theoretical studies.[7,8] The basic unit of LH-II is a heterodimer consisting of two small protein subunits referred to as the α- and β-apoproteins. The α heterodimers bind three bacteriochlorophyll (BChl) molecules, two of which are in close contact. These dimers form a ring (see Figure 1) that absorbs around 850 nm. The third BChl of the structural unit is located about 19 Å away on an outer ring whose absorption maximum lies at 800 nm. Carotenoid molecules in proximity to the outer BChl ring harvest light in a different spectral range and also prevent photooxidation of the chlorophylls. The LH-II of the above species is composed of eight or nine such units.

This article is concerned with the energy-transfer process within the inner ring of these LH-II systems. In the absence of static disorder, the eigenstates of the 16 singly excited BChl molecules of *Rs. molischianum* form two exciton bands. Only the degenerate second and third excited states carry oscillator strength, and thus, initial excitation at zero temperature should produce a delocalized linear combination of these. Femtosecond pumb−probe experiments have monitored the subsequent energy flow and found that intraband relaxation occurs within less than 50 fs at room temperature.[9−13] Whether the energy deposited in the ring remains delocalized under biological conditions is a matter of considerable debate. Static disorder, caused by structural inhomogeneity,[14−18] and also exciton−vibration coupling and temperature are factors expected to favor localization. The energy-transfer process within the LH-II system has been studied by fluorescence, transient absoprtion, and time-resolved fluorescence anisotropy techniques.[15,19,18,20,21] Because of the complexity of these systems, the interpretation of the measured superradiance and emission anisotropy has been elusive and the reported estimates of the coherence lengths vary from one to two subunits to a substantial portion of the ring. Some groups have reported evidence of delocalized states at all temperatures,[22−24] while the findings of others indicate incoherent energy transfer between monomers or dimers even under cryogenic conditions.[15,25] These apparent discrepancies have been attributed[26] to a strong temperature dependence of the superradiance enhancement factor not accounted for in the interpretation of these experiments. Theoretical investigations have assessed the effect of static disorder on the coherence of the exciton eigenstates in an isolated ring and found it to be small.[27] The effects of static and dynamic disorder on the resulting superradiance have been examined using adiabatic and polaron models.[28] Other recent work has employed a multilevel Redfield description to follow the dynamics of the photoexcited state in

* To whom correspondence should be addressed. Address: School of Chemical Sciences, University of Illinois, 601 S. Goodwin Avenue, Urbana, Illinois 61801.

10.1021/jp9917143 CCC: $18.00
Published on Web 11/25/1999

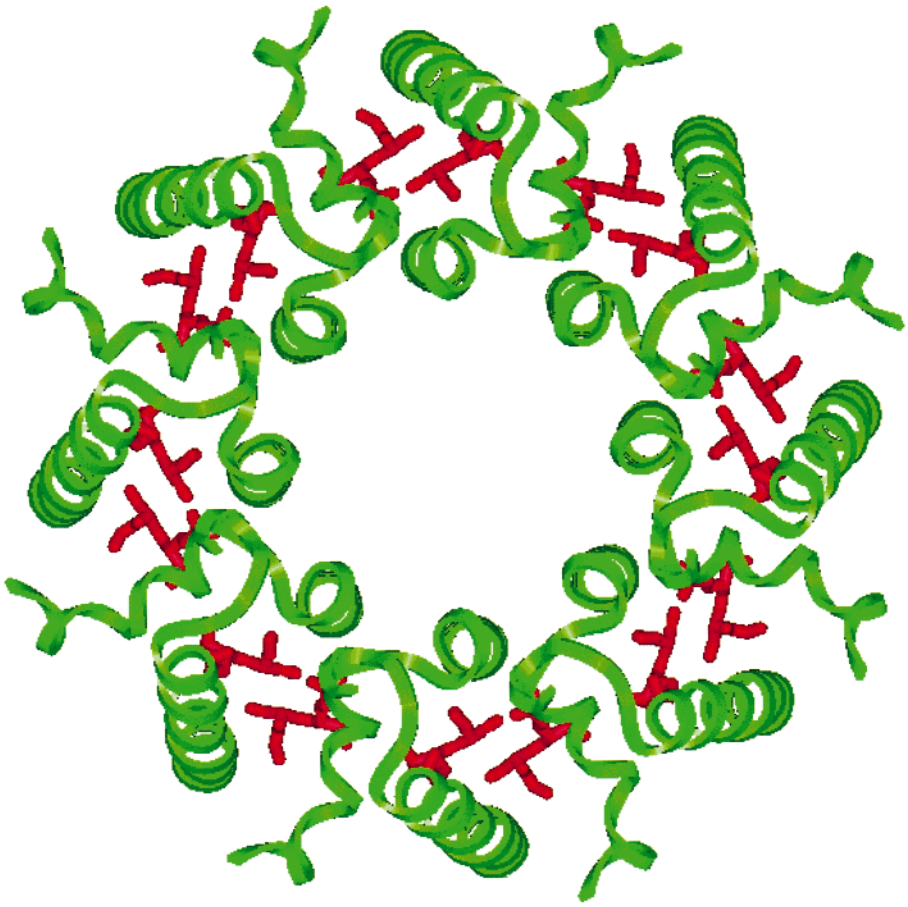

Figure 1. Top view of the B850 ring of the LH-II in *Rs. molischianum*. The 16 bacteriochlorophyll monomers are shown in red, while the α and β heterodimers are depicted in green.

the presence of coupling to vibrations modeled in terms of a dissipative bath and estimated the exciton coherence domain.[29−31]

In the present paper we adopt the imaginary time path integral formulation of quantum statistical mechanics[32] to investigate the equilibrium properties of the excited LH-II complex. The Monte Carlo path integral description of light-harvesting systems is appealing for several reasons: it can take into account the effects of ensemble averaging at a given temperature, exciton−vibration coupling, and static disorder automatically in a single calculation; in addition, it leads to simple pictures that allow easy visualization of the pertinent coherence length.

In section II we use a simple two-level-system paradigm to motivate the path integral analysis of the coherence length in LH-II. Section III describes the model and the discretized path integral representation of the quantum partition function, which we adopt. The results of our calculations are presented in section IV. That section reports the mean coherence length that we obtain as a function of temperature and dynamic disorder. Further, graphical representation of typical paths provides an intuitive picture of the coherence in the energy transfer. Finally, some concluding remarks are given in section V.

II. Theoretical Analysis

To motivate the calculation and facilitate the analysis of the results presented in the next section, it is instructive to consider the equilibrium distribution of an isolated two-level system (TLS). In the site representation the Hamiltonian reads

$$H = -\hbar\Omega(|L\rangle\langle R| + |R\rangle\langle L|) \tag{2.1}$$

where $|L\rangle$ and $|R\rangle$ are left- and right-localized states and the tunneling splitting is $2\hbar\Omega$. Coherences are associated with the off-diagonal elements of the density matrix in the site basis. To obtain a quantitative measure for the significance of these off-diagonal elements, we examine their contribution to the canonical partition function. The latter is given by the expression

$$Z = \mathrm{Tr}\, \mathrm{e}^{-\beta H} = \langle L|\mathrm{e}^{-\beta H}|L\rangle + \langle R|\mathrm{e}^{-\beta H}|R\rangle = 2\langle L|\mathrm{e}^{-\beta H}|L\rangle \tag{2.2}$$

where the last step follows from the symmetry of the Hamiltonian. By use of the path integral representation of the imaginary time propagator, this element takes the form

$$\langle L|\mathrm{e}^{-\beta H}|L\rangle = \sum_{k_1=L,R} \cdots \sum_{k_{N-1}=L,R} \langle L|\mathrm{e}^{-\beta H/N}|\sigma_{k_1}\rangle\langle\sigma_{k_1}|\mathrm{e}^{-\beta H/N}|\sigma_{k_2}\rangle\cdots\langle\sigma_{k_{N-1}}|\mathrm{e}^{-\beta H/N}|L\rangle \tag{2.3}$$

where $\sigma_k = L, R$ and N is the number of imaginary time steps. As is well-known, each realization $L, \sigma_{k_1}, \sigma_{k_2}, \ldots, \sigma_{k_{N-1}}, L$ of localized states defines a closed path. Coherence prevails if the paths that contribute most to the partition function alternate between the two sites. On the other hand, if most statistically significant paths are localized for the most part, the equilibrium distribution is characterized by lack of coherence.

To obtain a feel for the nature of the coherent and incoherent contributions, we examine the terms that enter the path sum for $N = 2$. We choose this particular value of N because it is the smallest value that allows paths to visit both accessible sites. A straightforward calculation leads to the following result for the contributions of localized vs delocalized paths:

$$\langle L|e^{-\beta H/2}|L\rangle\langle L|e^{-\beta H/2}|L\rangle = \left\{\frac{1}{2}e^{-\beta Eg/2}(1+e^{-\hbar\beta\Omega})\right\}^2 \quad (2.4a)$$

$$\langle L|e^{-\beta H/2}|R\rangle\langle R|e^{-\beta H/2}|L\rangle = \left\{\frac{1}{2}e^{-\beta Eg/2}(1-e^{-\hbar\beta\Omega})\right\}^2 \quad (2.4b)$$

From these expressions it follows that localized and delocalized paths make equal contributions to the partition function at zero temperature. In the opposite limit of infinite temperature the weight of the delocalized path vanishes and the partition function is dominated by paths that remain on one site.

We define the coherence length of a path as twice the root-mean-square deviation of the path from its centroid. Restricting attention to the above two types of paths, the mean coherence length (MCL) at a given temperature becomes

$$l = w_{\mathrm{loc}}\lambda_{\mathrm{loc}} + w_{\mathrm{deloc}}\lambda_{\mathrm{deloc}} \quad (2.5)$$

where w_{loc}, w_{deloc} are the weights of the localized and delocalized paths and λ_{loc}, λ_{deloc} are the corresponding lengths. In the TLS example one finds

$$l = \frac{d}{\sqrt{1+\gamma^2}} \quad (2.6a)$$

where d is the distance between left and right sites and

$$\gamma = \coth(\hbar\Omega\beta/2) \quad (2.6b)$$

Applying eq 2.6, one concludes that $l = 0$ at infinite temperature, while the zero temperature coherence length is found to be $l = d/\sqrt{2}$. Note that even at zero temperature the MCL is smaller than the site-to-site separation with the present definition. Other workers have adopted different measures where the MCL is defined as the inverse participation ratio or the autocorrelation function of the exciton wave function. Finally, at a temperature $\beta^{-1} = 2\hbar\Omega$ the TLS coherence length is $l \approx 0.24d$. Given that the population of the excited state is only 0.37 at this temperature, one might expect a higher degree of coherence. The reason for the short delocalization length predicted by eq 2.6 is the cyclic nature of equilibrium paths; as a consequence, the actual distance traversed by such a path is double the site-to-site distance.

III. Model and Computational Procedure

We model the photosynthetic antenna system by an n-state model in the basis of localized single excitations. This Hamiltonian is coupled diagonally to a dissipative heat bath comprising the vibrational and torsional modes of the pigments and their protein−water environment. In the absence of static or dynamic disorder the system is completely symmetric and takes the form

$$H_0 = \epsilon\sum_{i=1}^{n}|u_i\rangle\langle u_i| + \sum_{i\neq j}^{n}\Delta_{ij}|u_i\rangle\langle u_j| \quad (3.1)$$

where $n = 16$ for the B850 ring of LH-II in *Rs. molischianum*. Here, $|u_i\rangle$ denote single excitations of individual chlorophylls, ϵ is the corresponding excitation energy, and Δ_{ij} are the couplings that are due primarily to dipolar interactions. Symmetry implies that $\Delta_{2k+i,2k+j} = \Delta_{ij}$. Hu et al.[27] have parametrized this Hamiltonian by fitting the corresponding eigenvalues to results of ZINDO electronic structure calculations.[33] The resulting parameters are given in Table 1.

A qualitative description of the effects of exciton−vibration coupling on the dynamics of energy transfer is obtained by modeling the nuclear motion of the complex in terms of a dissipative bath of effective harmonic modes whose coordinates x_j are denoted collectively by the vector **x**. The harmonic bath picture is justified by virtue of the linear response approximation[34] as in the case of electron transfer.[35,36] The total Hamiltonian takes the form

TABLE 1: Parameterization of Eq 3.1 As Obtained by Hu et al.[a]

ϵ	13059
Δ_{12}	806
Δ_{23}	377
Δ_{13}	−152
Δ_{24}	−102

[a] All Parameters are in cm^{-1}

$$H = H_0 + \sum_{j=1}^{n}\frac{p_j^2}{2m_j} + \frac{1}{2}m_j\omega_j^2\left(x_j - \frac{c_j}{m_j\omega_j^2}\sum_{k=1}^{n}\sigma_k|u_k\rangle\langle u_k|\right)^2 \quad (3.2)$$

As is well-known, only the collective characteristics of the bath, rather than the individual mode frequencies ω_j and coupling constants c_j, affect the ring dynamics with this Hamiltonian. These collective features are contained in the spectral density

$$J(\omega) = \frac{\pi}{2}\sum_j\frac{c_j^2}{m_j\omega_j}\delta(\omega-\omega_j) \quad (3.3)$$

which can be obtained from the force−force autocorrelation function of the medium.[34,37,38] Since molecular dynamics calculations of the LH-II correlation function have not been reported, we employ a simple model of a generic Ohmic bath whose spectral density takes the form

$$J(\omega) = 2\pi\hbar\xi\omega\, e^{-\omega/\omega_c} \quad (3.4)$$

This function has a maximum at $\omega_c = 100\ \mathrm{cm}^{-1}$.[39,30] The reorganization energy between two adjacent chlorophyll monomers is related to the exciton−vibration coupling characterized by ξ through the expression

$$E_r = \frac{1}{\pi}(\sigma_k - \sigma_{k-1})^2\int_0^\infty\frac{J(\omega)}{\omega}\,d\omega = 2\hbar\xi\omega_c(\sigma_k - \sigma_{k-1})^2 \quad (3.5)$$

Given the unequal separations of neighboring chlorophyll monomers that belong to a single or to adjacent dimers, we expect the intra- and interdimer reorganization energies to have somewhat different values. Knowledge of these reorganization energies would uniquely determine the parameters ξ and σ_k that are needed to complete the model. A rough estimate of the reorganization energy can be obtained from the dynamic Stokes shift, which has been found[40,10] to be about 80 cm^{-1}. Ultrafast experiments[10] also revealed that the electronic excitations are coupled to nuclear motions with frequencies ranging from 20 to 1000 cm^{-1}. We thus choose $\omega_c = 100\ \mathrm{cm}^{-1}$. In the absence of more detailed information, we set σ_k equal to the chlorophyll monomer index k with periodic boundary conditions, i.e., $\sigma_{n+1} = \sigma_1$. We have verified that the coherence length reported in section IV remains essentially unchanged if a slightly nonuniform choice of σ_k is made. Finally, we present results for the values $\xi = 0.1$ and 0.25, which describe exciton−vibration coupling corresponding to reorganization energies equal to 20 and 50 cm^{-1}, respectively.

The off-diagonal coupling elements obtained by Hu et al. are likely to be too large.[41−43] For this reason we also report results

for couplings that have been scaled down compared to those given in Table 1 by a factor of 2.

The calculation is performed in the site basis u_k. The partition function is given by the expression

$$Z = \mathrm{Tr}\, e^{-\beta H} = \sum_{i=1}^{n} \int_{-\infty}^{\infty} d\mathbf{x}\, \langle u_i \mathbf{x}| e^{-\beta H} |\mathbf{x} u_i\rangle \qquad (3.6)$$

which is written in the discretized path integral representation:

$$Z = \sum_{k_1=1}^{n} \sum_{k_2=1}^{n} \cdots \sum_{k_N=1}^{n} \int_{-\infty}^{\infty} d\mathbf{x}_1 \int_{-\infty}^{\infty} d\mathbf{x}_2 \cdots \int_{-\infty}^{\infty} d\mathbf{x}_N \langle u_N \mathbf{x}_N| e^{-\beta H/N} |\mathbf{x}_{N-1} u_{N-1}\rangle \cdots \langle u_2 \mathbf{x}_2| e^{-\beta H/N} |\mathbf{x}_1 u_1\rangle \langle u_1 \mathbf{x}_1| e^{-\beta H/N} |\mathbf{x}_N u_N\rangle \qquad (3.7)$$

The imaginary time propagator is split symmetrically using the isolated exciton Hamiltonian as the reference:[44]

$$\langle u_i \mathbf{x}_i| e^{-\beta H} |\mathbf{x}_j u_j\rangle = \langle \mathbf{x}_i| e^{-[\beta/(2N)][H(\sigma_i) - H_0]} e^{-[\beta/(2N)][H(\sigma_j) - H_0]} |\mathbf{x}_j\rangle \langle u_i| e^{-\beta H_0/N} |u_j\rangle \qquad (3.8)$$

In turn, the isolated exciton propagator is calculated in terms of the eigenstates Φ_k and eigenvalues E_k of eq 3.1:

$$\langle u_i| e^{-\beta H_0/N} |u_j\rangle = \sum_{k=1}^{n} \langle u_i|\Phi_k\rangle\, e^{-\beta E_k/N} \langle \Phi_k| u_j\rangle \qquad (3.9)$$

With the present harmonic model for the nuclear vibrations, the integrals in eq 3.5 are of the Gaussian form and can be performed analytically. The result is[45]

$$Z = \sum_{k_1=1}^{n} \sum_{k_2=1}^{n} \cdots \sum_{k_N=1}^{n} \langle u_N| e^{-\beta H_0/N} |u_{N-1}\rangle \cdots \langle u_2| e^{-\beta H_0/N} |u_1\rangle \langle u_1| e^{-\beta H_0/N} |u_N\rangle\, F(\sigma_1, \sigma_2, \ldots, \sigma_N) \qquad (3.10)$$

where F is the influence functional and is given by the expression

$$F(\sigma_1, \sigma_2, \ldots, \sigma_N) = \exp\left(-\sum_{k=1}^{N} \sum_{k'=1}^{N} \eta_{kk'} \sigma_k \sigma_{k'}\right) \qquad (3.11)$$

The coefficients $\eta_{kk'}$ are given through integrals of the spectral density.

Because paths entering the path integral expression of the partition function are closed, these paths can be thought of as a necklace whose beads correspond to the auxiliary variables of eq 3.8.[46] In the present case each bead can occupy one of the n lattice sites of the LH-II ring. This correspondence allows straightforward visual examination of the system's coherence.

Paths contributing to eq 3.10 are sampled via a Metropolis procedure using the entire integrand as the sampling function. The coherence length of a path is obtained from the expression i.e.,

$$l = 2 \sum_{k_1=1}^{n} \sum_{k_2=1}^{n} \cdots \sum_{k_N=1}^{n} \langle u_N| e^{-\beta H_0/N} |u_{N-1}\rangle \cdots \langle u_2| e^{-\beta H_0/N} |u_1\rangle \langle u_1| e^{-\beta H_0/N} |u_N\rangle\, F(\sigma_1, \sigma_2, \ldots, \sigma_N) [(\sigma_1 - \sigma_c)^2 + (\sigma_2 - \sigma_c)^2 + \cdots + (\sigma_N - \sigma_c)^2]^{1/2} \qquad (3.12)$$

where σ_c is the centroid of the closed path $\{\sigma_1, \sigma_2, \ldots, \sigma_N\}$.

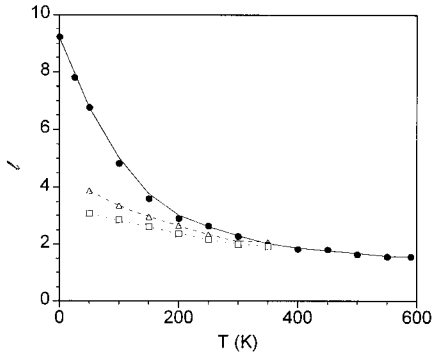

Figure 2. Coherence length as a function of temperature for the LH-II model with couplings from Table 1: (solid circles) isolated ring ($\xi = 0$); (hollow triangles) very weak exciton−vibration coupling ($\xi = 0.1$); (hollow squares) weak exciton−vibration coupling ($\xi = 0.25$). The lines are guides to the eye.

The effects of static diagonal disorder can be evaluated by replacing the parameter ϵ in eq 3.1 by the individual site energies ϵ_i, which are chosen from a Gaussian distribution with variance D. The MCL is then obtained from the ensemble average of l with respect to the fluctuation of the site energy. Interestingly, the integration associated with the inhomogeneous broadening of the ensemble can be combined with the Monte Carlo search for cyclic paths such that the effects of static disorder can be assessed within *a single random walk*. In this case the Boltzmann matrix elements of the reference Hamiltonian must be reevaluated for each choice of site energies.

In the next section we report the mean coherence length of the random walk and sketch typical paths for various parameters.

IV. Results

In this section we present the results of the path integral simulations described in section III. Figure 2 shows the coherence length in a 16-unit model of LH-II as a function of temperature for the isolated ring and also in the presence of small dissipation corresponding to $\xi = 0.1$ and $\xi = 0.25$. These calculations are performed without including disorder, using the coupling parameters of Table 1 for $N = 32$ path integral slices and 50 000 Monte Carlo points per integration variable after an equilibration step of equal length. At absolute zero the eigenstates are entirely delocalized. Dominant paths reflecting this delocalized structure exhibit coherence. The centroid of a completely delocalized path ($\sigma_k = \mathrm{int}(kn/N)$, $k = 1, \ldots, n$) is equal to

$$\sigma_c = \frac{n+1}{2} \qquad (4.1)$$

and (taking $N = n$ for simplicity), the coherence length is

$$l = 2\sqrt{\frac{1}{n}\sum_{k=1}^{n} (k - \sigma_c)^2} = \sqrt{\frac{1}{3}(n^2 - 1)} \qquad (4.2)$$

which for $n = 16$ equals 9.22. At low temperatures and in the absence of any disorder the system exhibits moderate coherence, reflecting the delocalized nature of the eigenstates. This is illustrated in Figure 3, which shows typical paths having coherence length within one unit of the calculated MCL at $T = 50$ K. Clearly, the delocalized exciton picture is relevant at or below this temperature. However, even in the case of an isolated,

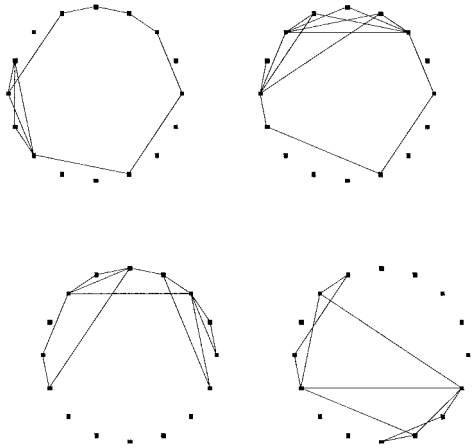

Figure 3. Typical paths for the isolated LH-II system ($\xi = 0$, no static disorder) at $T = 50$ K with the parameters shown in Table 1. The markers represent the chlorophyll monomers.

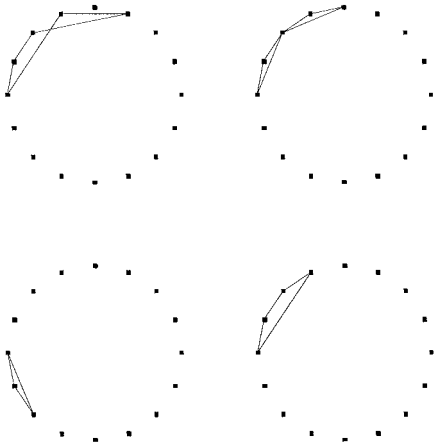

Figure 4. Typical paths for the isolated LH-II system ($\xi = 0$, no static disorder) at $T = 300$ K with the parameters shown in Table 1. The markers represent the chlorophyll monomers.

perfectly symmetric ring, only at very low temperatures does the path integral necklace begin to extend over the entire domain of the ring. As seen in Figure 2, thermal averaging has a dramatic effect on energy localization. At room temperature the coherence length is only 2.3 in the absence of any disorder. Typical paths at $T = 300$ K are shown in Figure 4. These paths now extend over only a few chlorophyll units. Note that these paths appear more delocalized than they actually are, since significant portions of the path integral necklace have collapsed on a single chlorophyll unit, an effect that cannot be discerned in the graphs. Coupling the ring to a weakly dissipative environment induces further localization, leading to $l = 2.1$ with $\xi = 0.1$ and $l = 2.0$ if $\xi = 0.25$ at 300 K. Still, coherence spans one to two dimers at room temperature, so hopping between individual monomers does not provide a faithful representation of energy transfer. At low temperatures where the perfect ring exhibits a high degree of coherence the effects of dissipation are more dramatic, as can be seen from Figure 2. Finally, inclusion of static disorder further enhances localization, although this effect is rather small, since the standard deviation of the site energies is small compared to the off-diagonal elements of the ring Hamiltonian.[27,47]

As alluded to in the previous section, the coupling parameters obtained by Hu et al. are deemed too large. For this reason we repeat the calculation of the MCL using coupling parameters that are scaled by a factor of $^1/_2$ with respect to those presented in Table 1. The resulting MCL is shown in Figure 5. Even

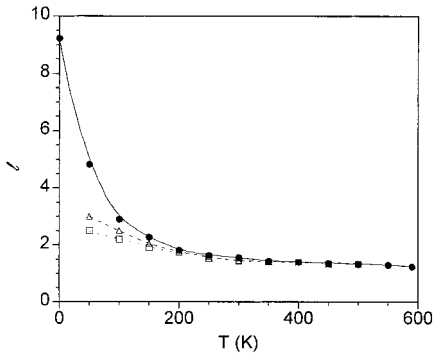

Figure 5. Coherence length as a function of temperature for the LH-II model with couplings from Table 1 scaled by 0.5: (solid circles) isolated ring ($\xi = 0$); (hollow triangles) very weak exciton−vibration coupling ($\xi = 0.1$); (hollow squares) weak exciton−vibration coupling ($\xi = 0.25$). The lines are guides to the eye.

though the MCL at zero temperature (where the ensemble is dominated by the ground state) is still given by eq 4.2, the MCL now decreases faster with increasing temperature and is equal to $l = 1.5$ at 300 K. The effects of dynamic disorder are again significant at low temperature, but given the very small extent of the paths at $T \geq 250$ K, this effect is negligible at room temperature.

From the results of these calculations it is evident that the coherence characterizing the exciton eigenstates of a perfect light-harvesting ring prevails only at very low temperatures. The calculated low-temperature MCL is in agreement with the estimate of Fleming and co-workers.[48] The major contributor to the localization observed at room temperature is thermal averaging, which destroys the coherent nature of individual eigenstates. Although static and dynamic disorder induce further localization, they are not crucial for disruption of coherence at biological temperatures. For this reason the conclusions reached on the basis of the simple model employing a harmonic dissipative bath appear robust and rather general.

In contrast to the localizing effects of the environment (temperature and static and dynamic disorder), the geometry of light-harvesting rings favors coherent energy transfer at low temperatures. Compared to a linear aggregate, the circular arrangement of the chlorophyll molecules eliminates the penalty in the Boltzmann factor associated with closing the path integral necklace for a path extending over at least half of the ring units. Choosing, for example, $N = n$, a completely delocalized path with $\sigma_k = k$, $k = 1, ..., n$ enters the partition function with exactly the same weight as the path

$$\sigma_k = k, \quad k = 1, ..., n/2$$
$$= n + 1 - k, \quad k = n/2 + 1, ..., n$$

This would not be the case if the pigments were arranged in an open shape. Since the coherence length of the first of these paths is larger, the overall MCL is increased. The geometric enhancement of coherence is modest under conditions that already favor delocalized paths, i.e., at low temperatures and weak disorder, but does not have an observable effect under biological conditions where coherence appears to span a small portion of the ring.

V. Concluding Remarks

In the absence of static disorder, the energy absorbed by the B850 ring of the LH-II system is used to excite a pair of degenerate exciton states that are delocalized over the entire

ring. However, coherence does not survive thermalization. At room temperature, the onset of thermal equilibrium is characterized by an incoherent ensemble of excitations that extend over two to three chlorophyll units. At very low temperatures coherence spans a significant portion of the ring and is enhanced by the circular arrangement of the pigments.

Although these conclusions were reached on the basis of a very simple model, they appear quite robust and insensitive to the details of the calculation. We employed the Hamiltonian of Hu et al. and a simple model for the effects of exciton−vibration coupling to describe the equilibrium properties of the LH-II ring. Despite the strong couplings in this parametrization, which certainly favor delocalization, we find that *at room temperature the coherence length is reduced by a factor of 4 with regard to the zero temperature case*. Our estimate of the room-temperature MCL is in reasonable agreement with the conclusions reached by the groups of van Grondelle[15,25] and Sundström,[2,28,30,31] who report a coherence domain of three to four monomers. If the couplings of the model are scaled down to more likely values, localization is even more pronounced. Addition of exciton−vibration coupling enhances localization. In the present work this coupling was modeled in terms of a dissipative harmonic bath. Although anharmonicity of the vibrational degrees of freedom may weaken the localizing effects of dynamic disorder, such motion should nevertheless destabilize extended states. It is thus hard to imagine the more intricate motion of the pigments and protein atoms resulting in a different outcome. Finally, if static disorder is also taken into consideration, the resulting MCL becomes even shorter. Thus, energy delocalization over the entire ring appears extremely improbable under biological conditions, although within a dimer and probably across two dimers coherence appears to prevail.

Acknowledgment. This material is based on work supported by the Research Corporation through a Cottrell Scholar Award and by the National Science Foundation through Award No. 93-57102. N.M. is grateful to the Director and the Faculty of the National Hellenic Research Foundation for their hospitality during her sabbatical leave from the University of Illinois.

References and Notes

(1) van Grondelle, R.; Dekker, J. P.; Gillbro, T.; Sundström, V. *Biochim. Biophys. Acta* **1994**, *1187*, 1−65.
(2) Pullerits, T.; Sundström, V. *Acc. Chem. Res.* **1996**, *29*, 381−389.
(3) Frank, H. A.; Cogdell, R. J. *Photochem. Photobiol.* **1996**, *63*, 257−264.
(4) Kühn, O.; Renger, T.; May, V.; Voigt, J.; Pullerits, T.; Sundström, V. *Trends Photochem. Photobiol.* **1997**, *4*, 213−256.
(5) *Resonance energy transfer*; Gnanakaran, S., Haran, G., Kumble, R., Hochstrasser, R. M., Eds.; John Wiley and Sons: Chichester, 1999; pp 308−365.
(6) Sundström, V.; Pullerits, T.; van Grondelle, R. *J. Phys. Chem. B* **1999**, *103*, 2327−2346.
(7) McDermott, G.; Prince, S.; Freer, A.; Hawthornthwaite-Lawless, A.; Papiz, M.; Cogdell, R.; Isaacs, N. *Nature* **1995**, *374*, 517.
(8) Hu, X.; Xu, D.; Hamer, K.; Schulten, K.; Koepke, J.; Michel, H. *Protein Sci.* **1995**, *4*, 1670−1682.
(9) Nagarajan, V.; Alden, R. G.; Williams, J. C.; Parson, W. W. *Proc. Natl. Acad. Sci. U.S.A.* **1996**, *93*, 13774.
(10) Kumble, R.; Palese, S.; Visschers, R. W.; Dutton, P. L.; Hochstrasser, R. M. *Chem. Phys. Lett.* **1996**, *262*, 396−404.
(11) Arnett, D. C.; Kumble, R.; Visschers, R. W.; Dutton, P. L.; Hochstrasser, R. M.; Scherer, N. F. Laser techniques for condensed phase and biological systems. *SPIE Proc.* **1998**.
(12) Freiberg, A.; Jackson, J. A.; Lin, S.; Woodbury, N. W. *J. Phys. Chem. A* **1998**, *102*, 4372−4380.
(13) Kennis, J. T. M.; Streltsov, A. M.; Permentier, H.; Aartsma, T. J.; Amesz, J. *J. Phys. Chem. B* **1997**, *101*, 8367−8372.
(14) Reddy, N. R. S.; Small, G. J.; Seibert, M.; Picorel, R. *Chem. Phys. Lett.* **1991**, *181*, 391−399.
(15) van Mourik, F.; Visschers, R. W.; v. Grondelle, R. *Chem. Phys. Lett.* **1992**, *193*, 1−7.
(16) Reddy, N. R. S.; Codgell, R. J.; Zhao, L.; Small, G. J. *Photochem. Photobiol.* **1993**, *57*, 35.
(17) Visschers, R. W.; van Mourik, F.; Monshouwer, R.; van Grondelle, R. *Biochim. Biophys. Acta* **1993**, *1141*, 238.
(18) Bradforth, S. E.; Jimenez, R.; van Mourik, F.; van Grondelle, R.; Fleming, G. R. *J. Phys. Chem.* **1995**, *99*, 16179.
(19) Pullerits, T.; Visscher, K. J.; Hess, S.; Sundström, V.; Freibert, A.; Timpmann, K.; van Grondelle, R. *Biophys. J.* **1994**, *66*, 236.
(20) Monshouwer, R.; van Grondelle, R. *Biochim. Biophys. Acta* **1996**, *1275*, 70−75.
(21) Hess, S.; Chachisvilis, M.; Timpmann, K.; Jones, M. R.; Fowler, G. J. S.; Hunter, C. N.; Sundström, V. *Proc. Natl. Acad. Sci. U.S.A.* **1995**, *92*, 12333−12337.
(22) Xiao, W. H.; Lin, S.; Taguchi, K. W.; Woodbury, N. W. *Biochemistry* **1994**, *33*, 8313−8222.
(23) Wu, H.-M.; Ratsep, M.; Lee, I.-J.; Cogdell, R. J.; Small, G. J. *J. Phys. Chem. B* **1997**, *101*, 7654−7663.
(24) Kennis, J. T. M.; Streltsov, A. M.; Aartsma, T. J.; Nozawa, T.; Amesz, J. *J. Phys. Chem.* **1996**, *100*, 2438−2442.
(25) Monshouwer, R.; Abrahamsson, M.; van Mourik, F.; van Grondelle, R. *J. Phys. Chem. B* **1997**, *101*, 7241−7248.
(26) Meier, T.; Chernyak, V.; Mukamel, S. *J. Phys. Chem. B* **1997**, *101*, 7332−7342.
(27) Hu, X.; Ritz, T.; Damjanovic, A.; Schulten, K. *J. Phys. Chem. B* **1997**, *101*, 3854−3871.
(28) Meier, T.; Zhao, Y.; Chernyak, V.; Mukamel, S. *J. Chem. Phys.* **1997**, *107*, 3876−3893.
(29) Kühn, O.; Sundström, V. *J. Phys. Chem. B* **1997**, *101*, 3432−3440.
(30) Kühn, O.; Sundström, V. *J. Chem. Phys.* **1997**, *107*, 4154−4164.
(31) Chachisvilis, M.; Kühn, O.; Pullerits, T.; Sundström, V. *J. Phys. Chem. B* **1997**, *101*, 7275−7283.
(32) Feynman, R. P. *Statistical Mechanics*; Addison-Wesley: Redwood City, CA, 1972.
(33) Cory, M. G.; Zerner, M. C.; Hu, X.; Schulten, K. *J. Phys. Chem. B* **1998**, *102*, 7640−7650.
(34) Makri, N. *J. Phys. Chem. B* **1999**, *103*, 2823−2829.
(35) Marcus, R. A.; Sutin, N. *Biochim. Biophys. Acta* **1985**, *811*, 265−322.
(36) Onuchic, J. N.; Wolynes, P. G. *J. Chem. Phys.* **1993**, *98*, 2218−2224.
(37) Warshel, A.; Hwang, J.-K. *J. Chem. Phys.* **1986**, *84*, 4938−4957.
(38) Schulten, K.; Tesch, M. *Chem. Phys.* **1991**, *158*, 421−446.
(39) Pullerits, T.; Van Mourik, F.; Monshouwer, R.; Visschers, R. W.; Van Grondelle, R. *J. Lumin.* **1994**, *58*, 168.
(40) Visser, H. M.; Somsen, O. J. G.; van Mourik, F.; Lin, S.; van Stokkum, I. H. M.; van Grondelle, R. *Biophys. J.* **1995**, *69*, 1083.
(41) Sauer, K.; Cogdell, R. J.; Prince, S. M.; Isaacs, N. W.; Scheer, H. *Photochem. Photobiol.* **1996**, *64*, 564.
(42) Pullerits, T.; Hess, S.; Herek, J.; Sundström, V. *J. Phys. Chem. B* **1997**, *101*, 10560−10567.
(43) Krueger, B. P.; Scholes, G. D.; Fleming, G. R. *J. Phys. Chem. B* **1998**, *102*, 5378−5386.
(44) Makri, N. *Chem. Phys. Lett.* **1992**, *193*, 435−444.
(45) Feynman, R. P.; Vernon, J. *Ann. Phys.* **1963**, *24*, 118−173.
(46) Chandler, D.; Wolynes, P. G. *J. Chem. Phys.* **1981**, *74*, 4078−4095.
(47) Wu, H.-M.; Reddy, N. R. S.; Small, G. J. *J. Phys. Chem. B* **1997**, *101*, 651−656.
(48) Jimenez, R.; Dikshit, S. N.; Bradforth, S. E.; Fleming, G. R. *J. Phys. Chem.* **1996**, *100*, 6825−6834.